Exploring printing methods for continuous natural fiber-reinforced thermoplastic biocomposites: A comparative study

Sustainable Materials and Technologies 43 (2025) e01253

Contents lists available at ScienceDirect

Sustainable Materials and Technologies

journal homepage: www.elsevier.com/locate/susmat

Exploring printing methods for continuous natural fiber-reinforced thermoplastic biocomposites: A comparative study

Natália V. dos Santos [a], Alberto Giubilini [b,c,*], Daniel Carlos T. Cardoso [a], Paolo Minetola [b,c]

[a] Department of Civil and Environmental Engineering (PUC-Rio), Marques de São Vicente Street, 225, Rio de Janeiro, RJ 22451-900, Brazil
[b] Department of Management and Production Engineering (DIGEP), Corso Duca degli Abruzzi 24, 10129 Turin, Italy
[c] Integrated Additive Manufacturing Centre (IAM@PoliTO), Politecnico di Torino, Corso Duca degli Abruzzi 24, 10129 Turin, Italy

ARTICLE INFO

Keywords:
Additive manufacturing
Fused filament fabrication
CFRTPCs
In-situ impregnation
Semi-finished filament

ABSTRACT

Continuous Fiber-Reinforced Thermoplastic Composites (CFRTPCs) are revolutionizing various industry sectors by enabling a combination of design, optimization, and high performance. The use of continuous natural fiber reinforcement integrates these factors with the potential for developing a sustainable product with a lower ecological footprint compared to tradition composites. However, challenges such as optimizing fiber-matrix impregnation and the identification of the most suitable manufacturing process for structural components remain significant. The objective of this study is to address these challenges by comparing the two main continuous printing methodologies - *in-situ* impregnation and semi-finished filament fabrication -in their application to natural fiber-reinforced composites. To achieve this, a method for manufacturing semi-finished filaments was developed and compared with the in-nozzle impregnation process by modifying a commercially available 3D printer. Image analysis, surface roughness measurements, deposition rates, and mechanical tests revealed that the semi-finished filament method resulted in better fiber-matrix impregnation, significantly improving tensile strength and elastic modulus by up to 18.4 % compared to the in-nozzle method. Additionally, the semi-finished filament process demonstrated a higher deposition rate, reaching 400 mm/s, compared to 300 mm/s for the in-nozzle process.

1. Introduction

Fused Filament Fabrication (FFF) stands as a cornerstone in additive manufacturing (AM), revolutionizing the production landscape with its capacity to construct intricately detailed and optimized components. By extruding thermoplastic filaments layer by layer, FFF enables the creation of complex geometries with precision and efficiency. However, FFF components face challenges with porosity and surface roughness. Porosity can arise from incomplete layer fusion, voids formed during extrusion, or the use of improperly dried filaments, all of which may compromise mechanical properties such as strength and durability [1,2]. Similarly, surface roughness, inherent to the layer-by layer process, can influence both the aesthetic quality and functional performance of FFF parts [3,4]. Despite these limitations, one interesting aspect of this technique is its versatility, allowing the incorporation of multiple materials within a single print. This capability not only broadens design possibilities but also enhances the structural performance and functionality of the final components. Furthermore, FFF promotes sustainability by significantly reducing waste generation compared to traditional fabrication methods [5].

Aligned with the pursuit of sustainability, incorporating natural fibers as filler and reinforcement agents in the 3D printing process has been gaining attention. Due to their lightweight nature, biodegradability, and mechanical resilience, these fibers have become increasingly popular in many sectors. Utilizing natural fibers not only aligns with eco-conscious practices but also enhances the overall performance and environmental footprint of the 3D-printed objects. As a result, this approach holds promise for fostering a more sustainable trajectory in AM processes. Table 1 shows the mechanical properties of the natural fibers most investigated in previous literature.

Natural fiber reinforcement can be incorporated in either discontinuous or continuous forms. Discontinuous fibers are generally used for manufacturing composite filaments, wherein a weight percentage of fibers is blended with the pellet matrix and extruded into filaments with dimensions compatible with market-available 3D printers [13]. The potential applications of Discontinuous Fiber-Reinforced Thermoplastic

* Corresponding author at: Department of Management and Production Engineering (DIGEP), Corso Duca degli Abruzzi 24, 10129 Turin, Italy.
E-mail address: alberto.giubilini@polito.it (A. Giubilini).

https://doi.org/10.1016/j.susmat.2025.e01253
Received 9 October 2024; Received in revised form 10 December 2024; Accepted 14 January 2025
Available online 20 January 2025

Table 1
Mechanical properties of natural fibers.

Type of fiber	Density (g/cm^3)	Tensile strength (MPa)	Elastic Modulus (GPa)	Reference
Bamboo	1.2	73–505	10–40	[6]
Coir	1.2–1.3	95–220	3–6	[6,7]
Curauá	1.4	500–1150	11.8	[8]
Flax	1.4–1.5	345–1500	28–80	[7,9,10]
Hemp	1.4–1.5	550–900	34–70	[6,7]
Jute	1.3–1.5	400–800	10–30	[7,8,11]
Kenaf	1.4	930	53	[9]
Ramie	1.5–1.6	400–968	44–128	[7,8,11,12]
Sisal	1.3–1.5	347–1150	9–38	[6–8,11]

Composites (DFRTPCs) include various sectors [14], including biomedical [15–17], design [18–21], and non-structural construction [22], due to their capacity for material recycling and ability to reuse waste materials [23]. Nevertheless, from a mechanical behavior perspective, the inclusion of discontinuous natural fibers often results in a reduction in the mechanical characteristics of the composite (Table 2).

The 3D printing methods using Continuous Fiber Reinforced Thermoplastic Composites (CFRTPCs) offer an effective option to improve the mechanical properties of components produced by FFF. Pervaiz et al. [29] pointed out three main types: semi-finished filament (SF), *in-situ* impregnation (IN), and out-of-nozzle printing (ON). In the SF approach, a composite filament is pre-manufactured by embedding the fiber in the matrix, to be used with conventional 3D printers [29]. However, this method limits flexibility in terms of material composition, as it imposes a fixed fiber volumetric fraction that cannot be modified during the printing process. The fiber content is entirely determined by the specifications of the pre-manufactured composite filament, making real-time adjustments impossible. Moreover, continuous fiber addition increases filament stiffness, leading to storage issues, especially in the case of stiffer fibers [30]. The IN method integrates the fiber into the polymer matrix during the 3D printing process. This integration within the printhead mechanism is achieved by feeding the fiber through an inlet or an auxiliary entrance in the coldend of the printhead, allowing to merge with the matrix before reaching the nozzle [29,30]. This method facilitates the variation of fiber volume ratio and allows the printing of pure filament and mixed fiber plastic and fiber parts. However, it requires special printhead modifications and is more likely to clog [11,29]. Lastly, the ON method uses two nozzles, one for the main polymer and another for the fiber reinforcement, which can be incorporated using either the SF [31,32] or IN [33] method. It is a versatile method that uses different fibers and matrices [29]. Table 3 summarizes the main studies of CFRTPCs, divided by insertion method.

Applying CFRTPCs with natural fibers poses a primary challenge concerning the utilization of yarn-form fibers, given that their natural length is discontinuous and inherently restricted by the size of the originating plant. The textile yarn is the final product of a long spinning process, where the final identification parameter is the yarn's title, which represents its diameter or thickness. In a simplified manner, fibers undergo cleaning following harvesting, alignment by carding and combing machines, regulated by draw frames, refinement through roving frames, twisting into yarns at the ring spinning mill, and packaging onto bobbins [48,49]. A major limitation in CFRTPCs processing is the difficulty in impregnating the fiber yarns effectively [11]. This phenomenon challenges the efficiency of the process, requiring innovative approaches to ensure the complete penetration of the thermoplastic polymer within the yarn.

Table 2
Mechanical properties of DFRTPCs using natural fibers. Adapted from [13].

Material	Fiber percentage (wt%)	Tensile strength (MPa)	Reference
PLA-Agave	0–10	51.0 (0 wt%) to 28.0 (10 wt%)	Figueroa-Velarde et al. [24]
PLA-Kenaf	0–7	56.3 (0 wt%) to 11.8 (7 wt%)	Shahar et al. [15]
PLA-Kenaf	0–2.5	49.9 (0 wt%) to 39.8 (2.5 wt%)	Haryati et al. [25]
PLA-Sugarcane	0–15	64.2 (0 wt%) to 45.3 (15 wt%)	Liu et al. [26]
PLA-Rubber	0–20	56.4 (0 wt%) to 34.3 (20 wt%)	Fekete et al. [27]
PLA-Soybean	0–10	36.4 (0 wt%) to 21.5 (10 wt%)	Dey et al. [28]

Although the in-nozzle method can be used with raw natural fibers [11,42], the fiber-matrix contact in the printing nozzle for a few seconds does not allow complete penetration [16], especially in the case of larger-diameter yarns for large-scale printing [11]. This uncompleted impregnation increases voids [11,42] and reduces mechanical properties [50]. To address this issue, various solutions have been reported, such as preheating the yarn before insertion in the printing nozzle [42] and the fiber's surface and sizing treatment [43,51]. Moreover, in semi-finished filaments, the composite is subjected to two heating processes: one during filament manufacturing and the second during deposition through the printing nozzle. However, this method also allows the presence of voids and irregularities in the composite [52], especially in larger yarns [53]. Treatments like coextrusion [32] and resin impregnation [53] are used to mitigate these issues. Coextrusion prepreg involves drawing continuous fibers into a single-screw pellet-extruder, while resin impregnation immerses continuous fibers in a resin impregnation tank.

A previous investigation developed a technique for continuous reinforcement using large diameter yarns with a modified FFF hotend, customized for *in-situ* impregnation of natural fibers within a biopolymer matrix for large-scale layers. This study assessed tensile properties and the applicability of the method to various natural fibers, emphasizing the importance of understanding fiber-matrix interfacial mechanical properties in CFRTPCs [11]. Nevertheless, a knowledge gap exists regarding the most effective continuous fiber printing method for continuous natural fibers in larger-scale diameters, both in mechanical terms and interface properties, to achieve enhanced characteristics of the novel biocomposite.

Despite growing interest in sustainable materials and their applications to FFF, the potential of reinforced structures using natural continuous fibers remains underexplored. This study addresses this challenge by comparing two continuous extrusion-based AM methods for CFRTPCs: *in-situ* impregnation and semi-finished filament fabrication. The novelty lies in the development of a method for manufacturing semi-finished filaments and the customized modification of a commercially available FFF 3D printer to produce in-nozzle impregnated samples. This setup, for the first time, enables a direct comparison of these approaches in terms of fiber impregnation, mechanical and thermal properties, and printing efficiency. This research explores flax yarns in a PLA matrix, focusing on how large-diameter continuous fibers affect material performance. PLA and flax yarns offer a sustainable and cost-effective solution. In fact, PLA filament costs around 20 €/kg, while flax yarns are priced at approximately 10 €/kg, significantly cheaper than carbon or glass fibers. Additionally, flax is renewable, biodegradable, and lightweight, enabling to partial biopolymer replacement in the final biocomposite, thus reducing both polymer usage and component cost.

By combining mechanical testing with image analysis, this study provides a deeper understanding of how 3D printing processes impact final material properties, offering valuable contributions to the development of sustainable, high-performance composites in FFF.

Table 3
CFRTPCs insertion methods using natural fibers. Adapted from [16].

Method		Reference	Matrix	Fiber
Semi-finished filament (SF)	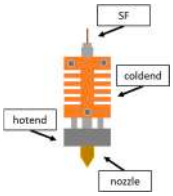	Le Duigou et al. [34,35]	PLA	Flax
		Fruleux et al. [36,37]	PLA	Flax
In-situ impregnation (IN)	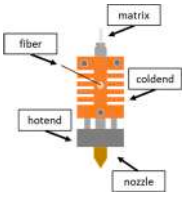	Cheng et al. [38–40]	PLA	Ramie
		Suteja et al. [41]	PLA	Pineapple leaf
		Matsuzaki et al. [42]	PLA	Jute
		Long et al. [43]	PLA	Flax
		Santos et al. [11]	PLA	Sisal, ramie and jute
		Cai et al. [44]	PLA	Ramie
		Terekhina et al. [45]	PA 6	Flax
		Rivero-Romero et al. [46]	PLA	Banana
Out-of-nozzle printing (ON)	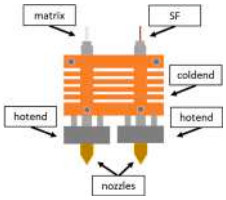	Zhang et al. [31,32]	PLA	Flax
	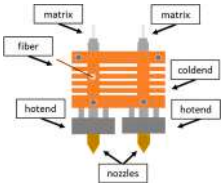	Ginoux et al. [33]	PLA	Hemp
		Wu et al. [47]	PLA	Flax

2. Materials and methods

2.1. Materials

The reinforcing materials used in this work consisted of flax yarn supplied by Bricolino (Vicenza, Italy) (Fig. 1). A polylactic acid filament (PLA 3D850) with a diameter of 1.75 mm and PLA pellets (SMARTFIL PLA) provided by Smar Materials 3D (Jaén, Spain) were used for the matrix. Table 4 presents the main properties of the natural yarn from literature and PLA from producer data sheet, respectively.

2.2. Printing fabrication

2.2.1. Semi-finished filament (SF)

To produce the semi-finished filaments reinforced with continuous natural fibers, modifications were made to the nozzle of the single-screw extruder, model NEXT 1.0 from 3Devo (Utrecht, Netherlands), to enable simultaneous extrusion of both the matrix and the reinforcement. The key components of the single-screw extruder, are depicted in Fig. 2a.

The fabrication of filaments depends on key parameters such as temperature, extruder speed, and puller speed. Fig. 2b illustrates a schematic diagram of the single-screw extrusion process. Temperature control within the single-screw extruder is divided into three distinct

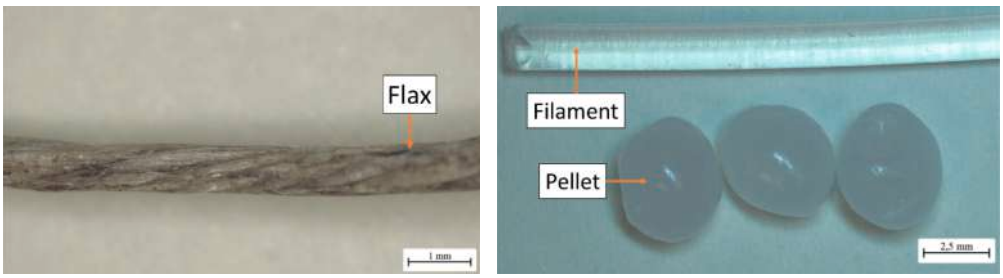

(a) (b)

Fig. 1. Matrix and reinforcement materials: (a) Natural fibers and (b) PLA matrix (Leica MSV266 optical microscope).

Table 4
Properties of the natural yarns and polymer matrix [7,8,10,11,54].

Property	Flax yarn	PLA 3D850	Smartfil PLA
Type	Yarn	Filament	Pellet
Diameter (mm)	0.77 ± 0.03	1.75	–
Density (g/cm^3)	1.4–1.5	1.24	1.24
Linear density (g/m)	0.50 ± 0.01	–	–
Tensile strength (MPa)	345–1500	57.7	110
Young modulus (GPa)	28–80	2.64	3.31
Ultimate strain (%)	–	3.10	–
Cellulose (%)	65–80	–	–
Hemicellulose (%)	12–16	–	–
Lignin content (%)	2–5	–	–
Moisture absorption (%)	7	–	–
Melting temperature (°C)	–	205–220	200–240

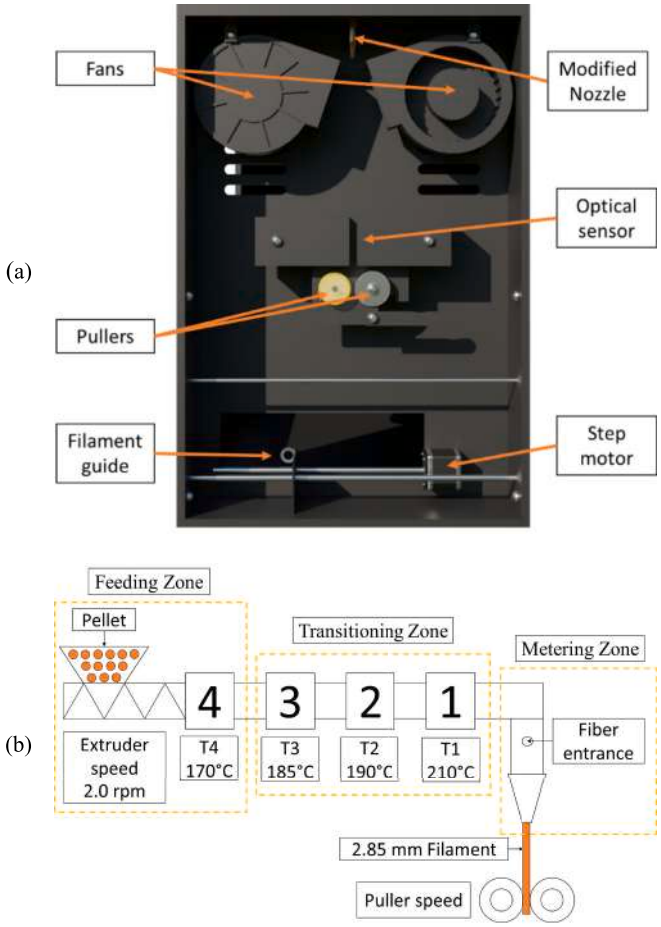

Fig. 2. Single-screw extruder: (a) schematic representation of the components; (b) schematic diagram of the process adapted from the manufacturer's design [55].

zones: feeding, transitioning, and metering. Each of these zones plays a pivotal role in ensuring consistent filament circularity and diameter during production [56].

In the feeding zone, the extruder speed determines the flow of material produced, and the temperature (T4) is linked to the viscosity of the material, requiring a minimum viscosity to avoid clogging the equipment. Along the transitioning zone, the temperatures T3 to T1 and flow pressure create a homogeneous material, avoiding bubbles and voids. Low temperatures within the nozzle can result in bubble formation and blockages, whereas excessively high temperatures may compromise the workability of the filament. Finally, the metering zone regulates the puller speed by the filament diameter, measured by the optical sensor.

The main modification of the machine occurred in the nozzle, which was replaced with a longer one with a specific hole to allow the entrance of the natural yarn, as shown in Fig. 3a. Fig. 3b, on the other hand, depicts a moment during the extrusion of the biocomposite filament. The extrusion parameters of the semi-finished filament are presented in Table 5.

2.2.2. *In-situ impregnation (IN)*

Modifications for *in-situ* impregnation were implemented in the Ender 3 V2 printer (Fig. 4), drawing inspiration from the work of Santos and Cardoso [11]. A 2 mm diameter hole was drilled into the coldend section of the extruder to facilitate impregnation. Additionally, alterations were made to the fan-fixing case to enable the insertion of yarn without requiring the removal of the extruder.

2.2.3. *Printing nomenclature*

The test nomenclature was defined to capture the effects of fiber addition, printing method, and matrix format utilized. The two printing methods were *in-situ* and semi-finishing, while the matrix formats used were filament and pellet. Table 6 presents the terminology used for each combination, clarifying the specific conditions studied.

3. Samples characterization

3.1. *Roughness test*

The roughness tests were performed using an ATOS Compact Scan (Zeiss, Oberkochen, Germany) in the Reverse Laboratory (Polito, Piemonte, Italy). The testing protocol followed the recommendations of ISO 4288 [57]. The specimens display 20 mm × 15 mm × 3.0 mm of geometry, prepared with a double layer containing continuous filaments with fibers oriented in the loading direction, with the same printed geometry characteristics of the tensile test samples. For each of the five conditions studied, measurements were taken at three distinct sections on each sample, and the average roughness was calculated. The roughness values were obtained from the upper profiles of the cross-sections of the samples. Fig. 5 illustrates the method used to acquire these measurements. This testing was conducted to analyze the surface of the printed material, highlighting the effects on layer interconnection and understanding the implications for interface bonding.

3.2. *Deposition rate test*

The deposition rate tests were analyzed using an Ender 3 V2 printer available in the Rapid Manufacturing Laboratory (RMLab) in the Integrated Additive Manufacturing Center (IAM@PoliTO, Turin, Italy). The printed samples were produced at varying speeds, ranging from 100 mm/min (S100) to 500 mm/min (S500), or until detachment of the composite from the print bed occurred. A constant temperature was maintained in all cases to ensure consistent yarn impregnation by the matrix. Fig. 6 provides a detailed illustration of the schematic path and schematic configuration for evaluating deposition rate and speed. Fig. 6a depicts the printing path on the print bed (x and y axes with dimensions of 230 mm), where successive serpentine lines are deposited at incrementally increasing speeds. The process begins at 100 mm/min (denoted as S100) and increases by 100 mm/min with each subsequent line, culminating at 500 mm/min. Fig. 6b complements this by showing an image of the actual 3D printing process, offering a visual representation of the test setup. Four tests were conducted for each practical condition (*i.e.*, IN-F and SF), and the printing properties are summarized in Table 7.

3.3. *Tensile test*

The tensile tests were conducted using an Aura 10 T universal testing machine from Easydur (Arcisate, Italy). An independent strain

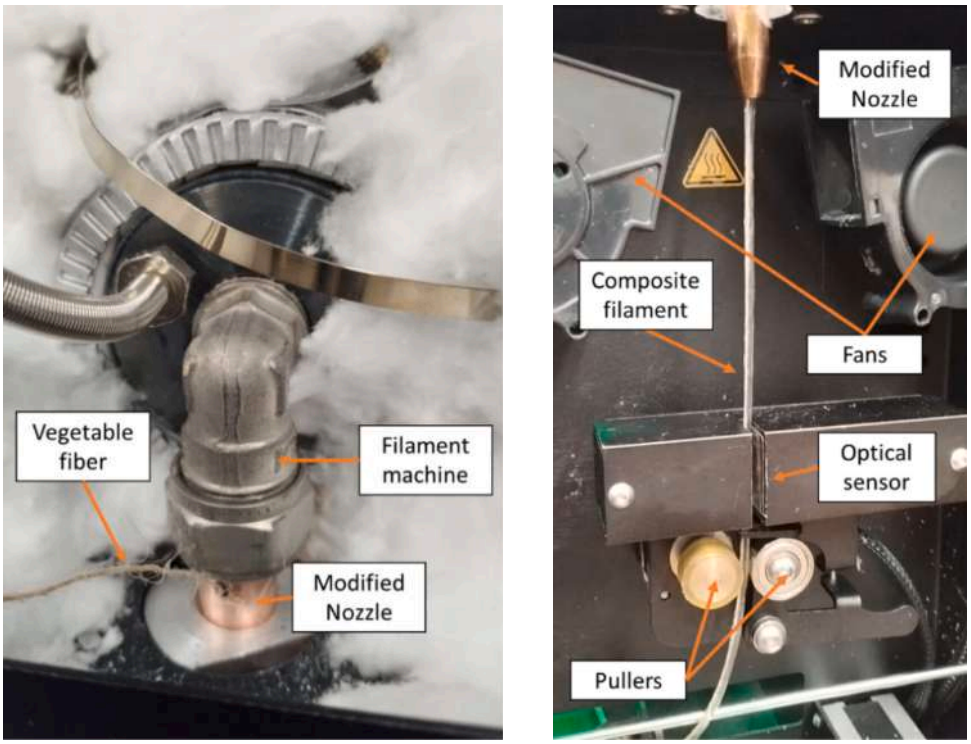

Fig. 3. Fabrication of Semi-finished Filament: (a) Fiber insertion into the modified nozzle, (b) semi-finished filament extrusion process.

Table 5
- Single-screw extruder settings.

Property	Value
T1 (°C)	210
T2 (°C)	190
T3 (°C)	185
T4 (°C)	170
Extruder speed (rpm)	2.0
Filament fan (%)	25
Filament diameter (mm)	2.85 ± 0.15
Spooling speed	automatic

measurement was conducted with an external X-Sight 2000 series optical extensometer (X-Sight s.r.o, Brno, Czech Republic), available in the Department of Management and Production Engineering (Polito, Turin, Italy). Fig. 7 illustrates the experimental setup for tensile characterization, including a specific representation of the tensile-tested samples. The testing protocol followed the recommendations of ASTM D3039 [58]. The tests were performed under displacement control at a rate of 5 mm/min until failure. The specimens, with dimensions of 220 mm × 28 mm × 3.0 mm, were prepared with a double layer of continuous filaments containing flax yarns aligned in the loading direction. Five samples were tested for each condition, with the printing parameters kept the same for both examined approaches and consistent with those used in the detachment test, detailed in Table 7. Based on the results of the deposition test, a printing speed of 200 mm/min was selected. To ensure a fair comparison between the 3D printing methods, the same printing parameters were applied to both approaches. While the optimal parameters for each method may differ, the chosen parameters were standardized across both methods to provide a comparison of approaches, with consistent 3D printing parameters.

3.4. Differential scanning calorimetry (DSC)

The DSC test was carried out using a NETZSCH DSC 200F3 Maia equipment, available in the LADES (CEFET/RJ, Rio de Janeiro, Brazil). The experiment was conducted with a heating rate of 20 K/min over a temperature range of 40–220 °C, under a nitrogen (N_2) flow of 50 mL/min. Approximately 20 mg of each sample were analyzed, following ASTM D3418 procedures [59]. The test aimed to determine the glass transition temperature (T_g), crystalline melting temperature (T_m), and factors such as the degree of crystallinity. In the context of this research, DSC was employed to evaluate the thermal effects of each printing method on the final crystallinity and enthalpy of the material. The enthalpy, which indicates the process's influence on the composite's crystallinity, is determined by the area under the exothermic peak in the DSC curve. Additionally, the degree of crystallization can be calculated using Eq. (1) as reported by Kong et al. [60].

$$X_c = \frac{\Delta H_m - \Delta H_{cc}}{\Delta H^o_m} \times 100 \quad (1)$$

where,

X_c- The weight fraction extent of crystallinity.

ΔH_m - The enthalpy of melting.

ΔH_{cc} - The enthalpy of cold crystallization.

ΔH^o_m - The enthalpy is the theoretical melting enthalpy of a purely crystalline PLA which was assumed to be equal to 93 J/g [61].

3.5. Scanning electron microscopy (SEM) analysis

The cross-sections of the specimens were analyzed using a TESCAN CLARA Scanning Electron Microscope (SEM), available at the Rheology Group (Greo) (PUC-Rio, Rio de Janeiro, Brazil). The equipment operated at 2 keV. Prior to analysis, the samples were dried in an oven at 60 °C for 24 h and stored in a desiccator to minimize moisture content. To enhance conductivity, the samples underwent a metallization process, in

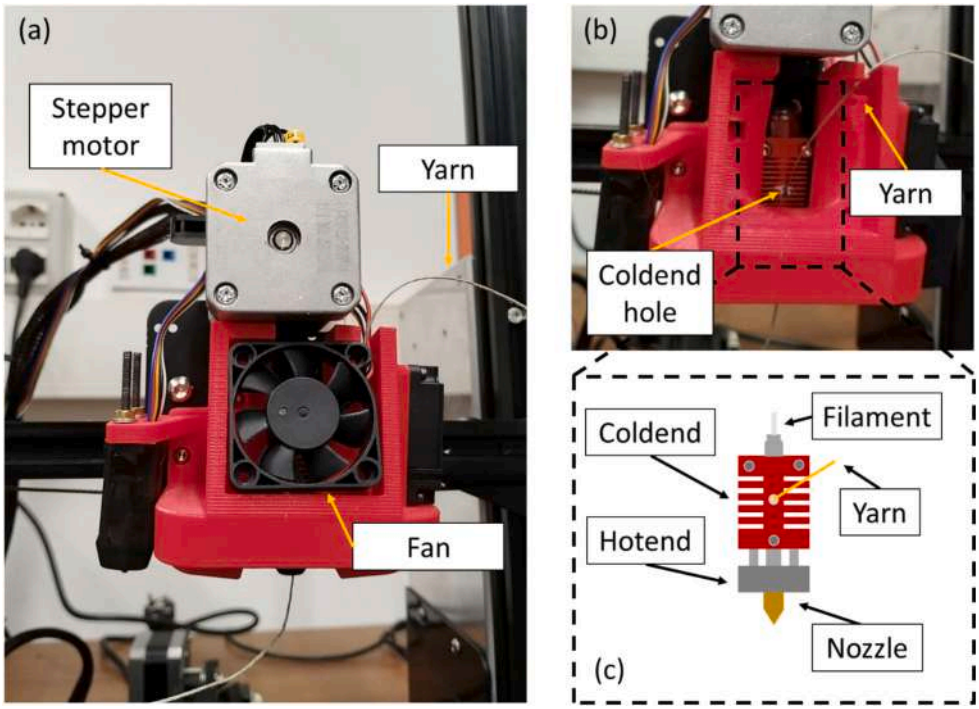

Fig. 4. Printer modification to *in-situ* printing: (a) Extruder, (b) fiber-entrance detail, and (c) schematic drawing.

Table 6
CFRTPCs' terminology.

Nomenclature	Presence of flax yarn	Type of PLA	Method
PLA-F	No	Filament	*In-situ*
IN-F	Yes	Filament	*In-situ*
PLA-P	No	Pellet	*In-situ*
IN-P	Yes	Pellet	*In-situ*
SF	Yes	Pellet	Semi-finished

which they were coated with a thin layer of gold.

4. Results and discussion

4.1. Effects of temperature and speed parameters on filament and printing quality and efficiency

The primary physical parameters influencing both filament production and 3D printing are temperature and speed. During filament manufacturing with a single-screw extruder, the key parameters governing quality control include extruder temperature, extrusion speed, and fan speed. Temperature is a critical factor influencing the viscosity of the material during extrusion. Lower temperatures result in

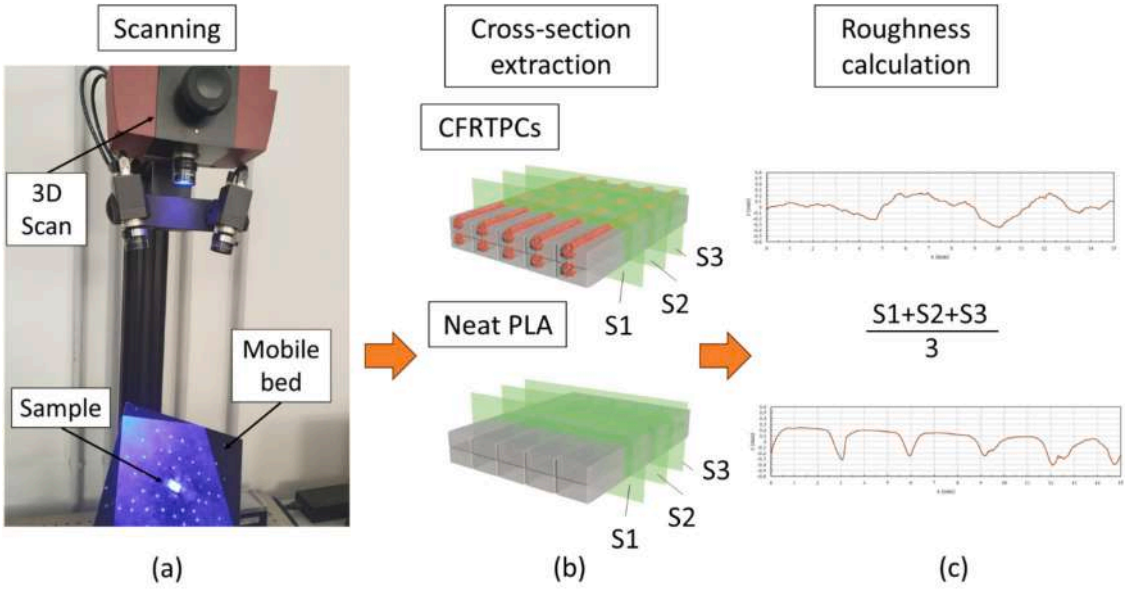

Fig. 5. Schematic representation of the surface roughness characterization method: (a) Scanning, (b) cross-section extraction, and (c) roughness calculation.

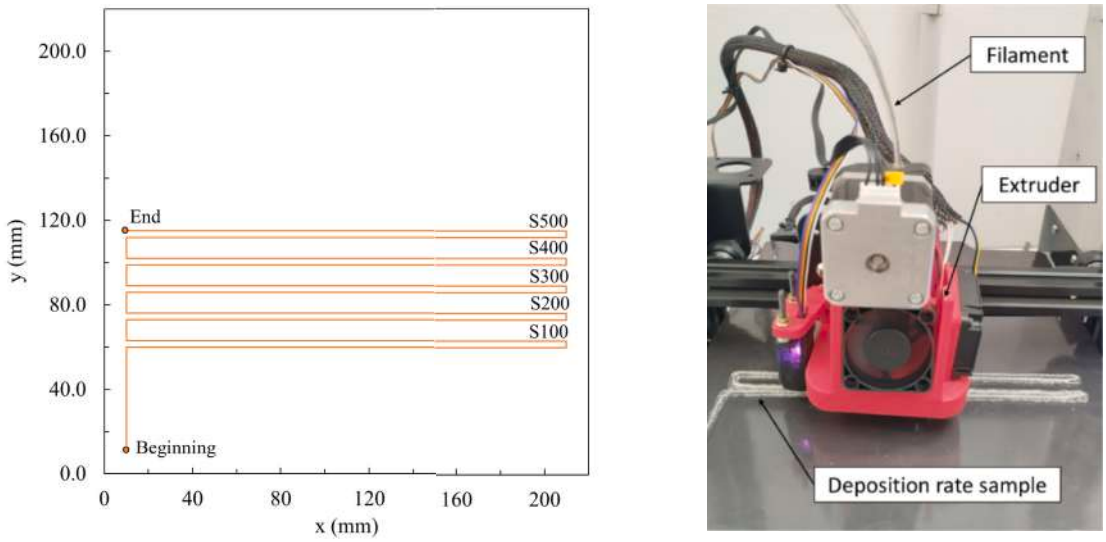

Fig. 6. Deposition rate test: (a) Schematic of path and speed configuration and (b) printing process.

Table 7
Deposition rate test's printing parameters.

Property	Value
Nozzle diameter (mm)	2.0
Speed range (mm/min)	100–500
Extruder temperature (°C)	200
Bed temperature (°C)	60
Layer height (mm)	1.5
Layer width (mm)	3.0

excessively high viscosity, which increases resistance to flow and can cause air entrapment, leading to bubble formation within the filament (Fig. 8a). Conversely, higher temperatures can excessively reduce viscosity, preventing the polymer from achieving the necessary consistency to form a filament with the required diameter (Fig. 8b). For PLA, the optimal working temperature range is between 180 °C and 220 °C. When incorporating thicker yarns, a higher temperature, within the material's workable limits, is selected to achieve superior impregnation. In this study, a temperature of 210 °C was employed to ensure optimal yarn impregnation within the filament matrix.

Fig. 9a shows a representation of the obtained semi-finished filament produced with a diameter of 2.85 ± 0.15 mm and a fiber volumetric fraction of 13.5 %. The variation in filament diameter, approximately 0.15 mm or around 5 %, observed in the extrusion of pellets reinforced by natural fibers, is attributed to internal flow variations within the filament extruder, as reported in other works in the literature [13]. Fig. 9b presents an optical micrograph of a cross-section of the obtained biocomposite filament, where it is possible to note the non-uniform distribution of fibers, as an inherent consequence of the CFRTPCs process. As a matter of fact, during extrusion, the flow of the molten composite material exerts a drag force on the fibers, which partially displaces them from the deposited line, leading to misalignment. This behavior, which results in fiber distribution irregularities, has been

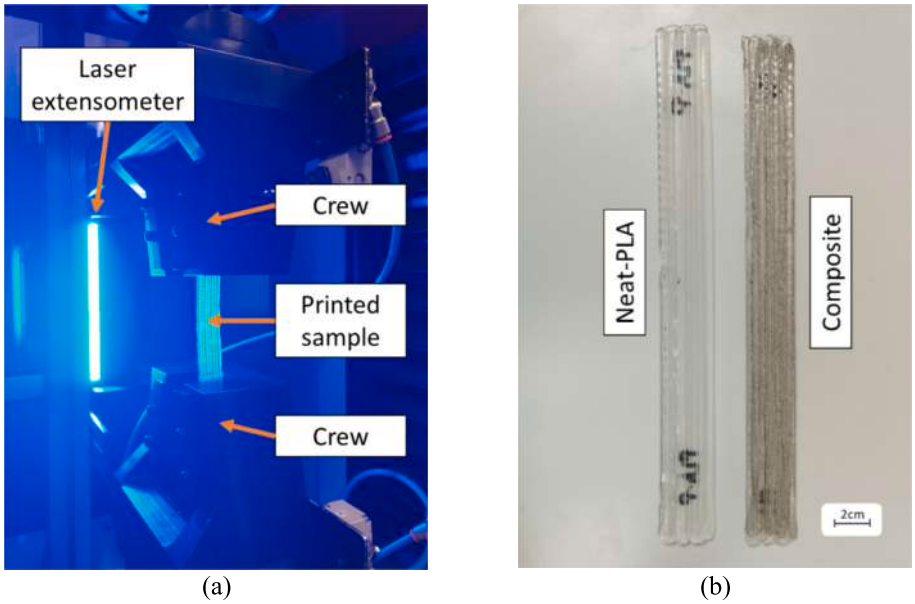

Fig. 7. Photographs of the tensile testing: (a) Analysis setup and (b) 3D printed samples.

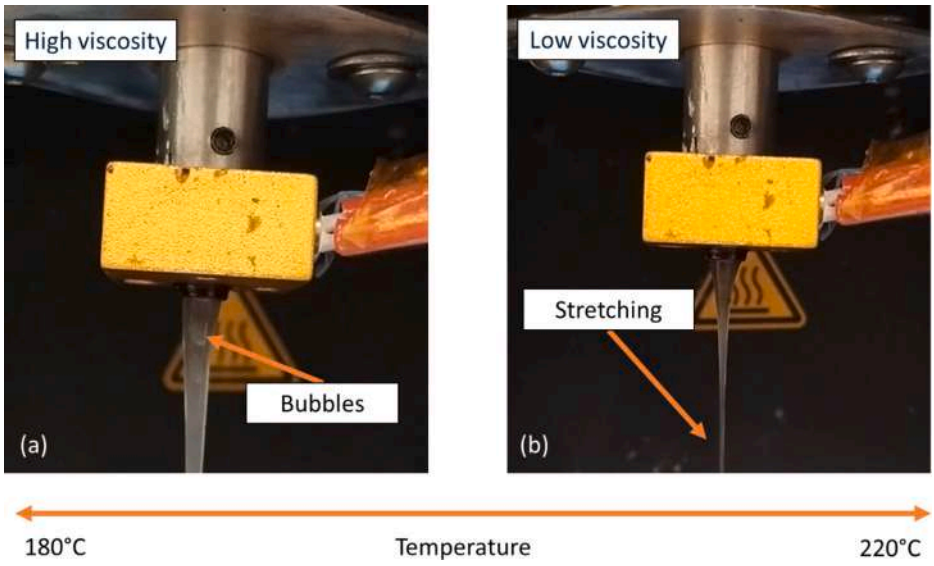

Fig. 8. Filament fabrication temperature with two distinct issues: (a) low viscosity and (b) high viscosity.

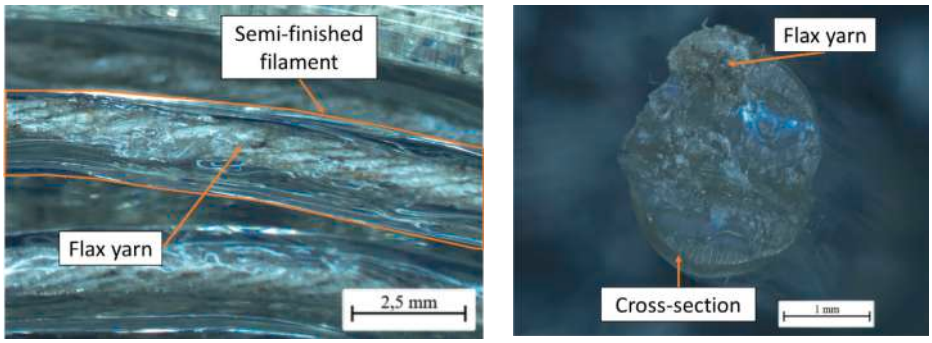

Fig. 9. Semi-finished filaments: (a) Photograph of a semi-finished flax filament, (b) Micrograph of biocomposite filament cross-section.

previously observed by Rivero-Romero et al. [46] and Cheng et al. [38]. Further process optimization may help mitigate this issue, but it remains a challenge associated with the current filament fabrication technique.

In the filament manufacturing process, the addition of continuous yarn introduces several effects. These include yarn eccentricity within the filament (Fig. 10a), the presence of inherent material impurities (Fig. 10b), variations in the cross-section dimensions (Fig. 10c), and regions lacking sufficient impregnation (Fig. 10d). Yarn eccentricity (Fig. 10a) is also observed in SF printing, as it occurs in the IN-F process. In these cases, it is due to the stresses generated during 3D printing, where the yarn is tensioned between the fixed part on the print bed and the impregnated part inside the extruder.

Similarly, high extruder speeds result in inconsistent flow and increased bubble formation, which consequently reduces the quality of the printing filament. This necessitates balancing the optimal polymer extrusion speed with the energy consumption required for its production. In this research, a speed of 2.0 rpm was selected for composite fabrication, as the introduction of fibers increases the bubble formation rate, requiring more precise control of the flow.

The printing speeds of the two methods (SF and IN) may be constrained by the specific process employed. In the IN method, the yarn is pulled through friction between the matrix and the reinforcement, allowing for some variation in matrix flow during printing, as the fiber moves more freely. In contrast, in the SF method, both the matrix and reinforcement are uniformly pushed by a stepper motor, limiting flow variation due to the fixed filament volume. Consequently, the SF method requires specific flow conditions (Fig. 11). Reduced flow rates can lead to persistent fiber fractures, negatively impacting overall continuity, while excessive flow rates may result in material curling due to over-extrusion. The optimal flow condition involves depositing the yarn in a single, consistent, and linear manner.

Finally, in the deposition rate test, where printing speeds ranging from 100 to 500 mm/min were tested under consistent bed and nozzle temperatures, the outcome of continuous yarn printing using SF impregnation revealed a clear dependence on optimal flow. Fig. 12 presents the outcomes of the deposition rate tests for the SF (Fig. 12a) and IN methods (Fig. 12b). The maximum speeds at which detachment was avoided for SF and IN-F were 400 mm/min and 300 mm/min, respectively, showing a 33.3 % increase in maximum printing speed when the yarn was pre-impregnated into a single composite filament. This improvement can be attributed to the SF method, which may reduce pre-tension in the yarn during deposition, as the stepper motor extrudes both the matrix and fiber reinforcement uniformly.

4.2. *Evaluation of fiber impregnation and composite roughness*

The roughness of fiber insertion was analyzed using different methods to determine the main effects of each process. Fig. 13 and Table 8 show the roughness curves and measured parameters for each process. Comparing PLA-F and PLA—P, the matrix produced from pellets

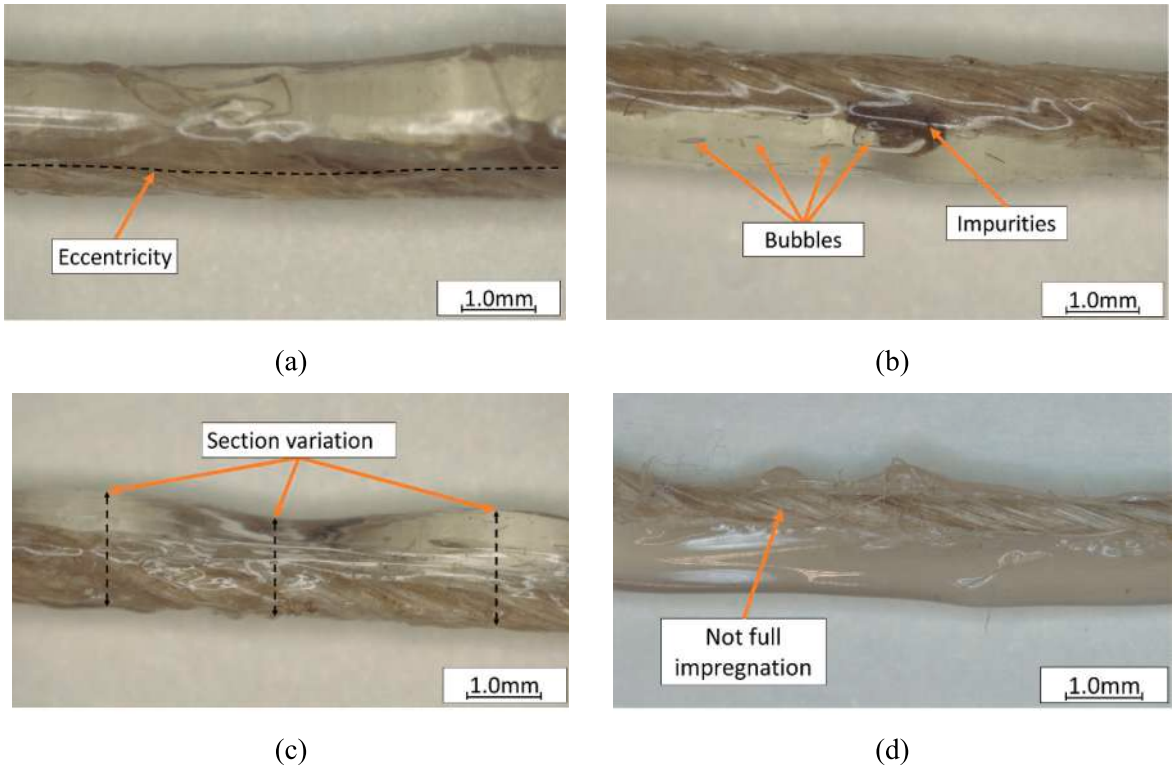

Fig. 10. Composite filament manufacturing problems: (a) Eccentricity of the fiber, (b) impurities and bubbles, (c) section variation, and (d) not complete impregnation.

Fig. 11. Flow variation in the deposition rate test of flax composite filaments.

(PLA—P) exhibited greater uniformity between layers (Fig. 13b). However, this uniformity resulted in lower inter-layer adhesion, as evidenced by a higher surface roughness for PLA-P (Ra^{PLA-P}=0.170 ± 0.008 mm) compared to PLA-F (Ra^{PLA-F}=0.071 ± 0.000 mm). This trend is further supported by the amplitude parameters: Rq (Rq^{PLA-F}=0.085 ± 0.000 mm and Rq^{PLA-P}=0.217 ± 0.005 mm) and Rz (Rz^{PLA-F}=0.336 ± 0.026 mm and Rz^{PLA-P}=0.960 ± 0.120 mm).

Some phenomena were observed when inserting the fiber reinforcement. Using commercial filament and the in-nozzle method (IN-F), there was a 100 % increase in roughness (Ra^{PLA-F}=0.071 ± 0.000 mm and Ra^{IN-F}=0.142 ± 0.019 mm), approximately a 116 % increase in amplitude (Rz^{PLA-F}=0.336 ± 0.026 mm and Rz^{IN-F}=0.725 ± 0.026 mm), and an increase in Root Mean Square (RMS) roughness inherent in the combination of these materials.

In the case of pellet-based matrix, the reinforcement reduced roughness by 5.8 % for the in-nozzle method (Ra^{PLA-P}=0.170 ± 0.008

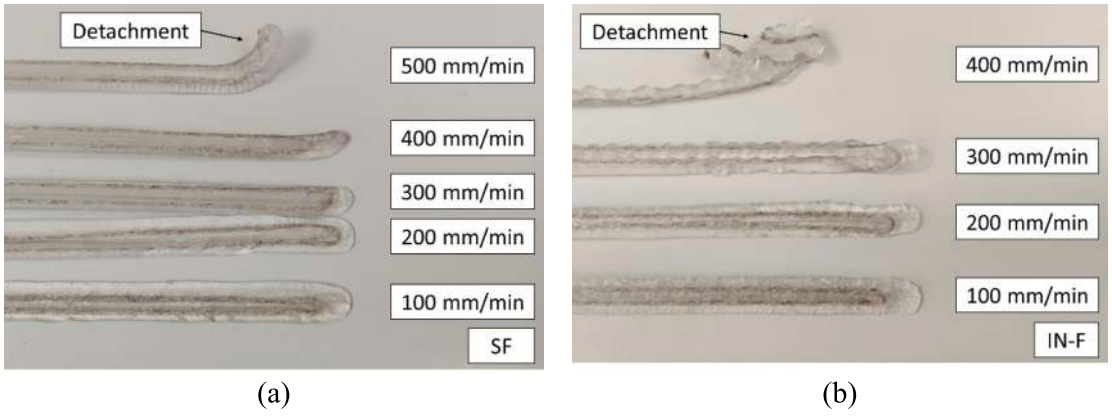

Fig. 12. Photographs of deposition rate test results for the two configurations: (a) SF method, (b) IN-F method.

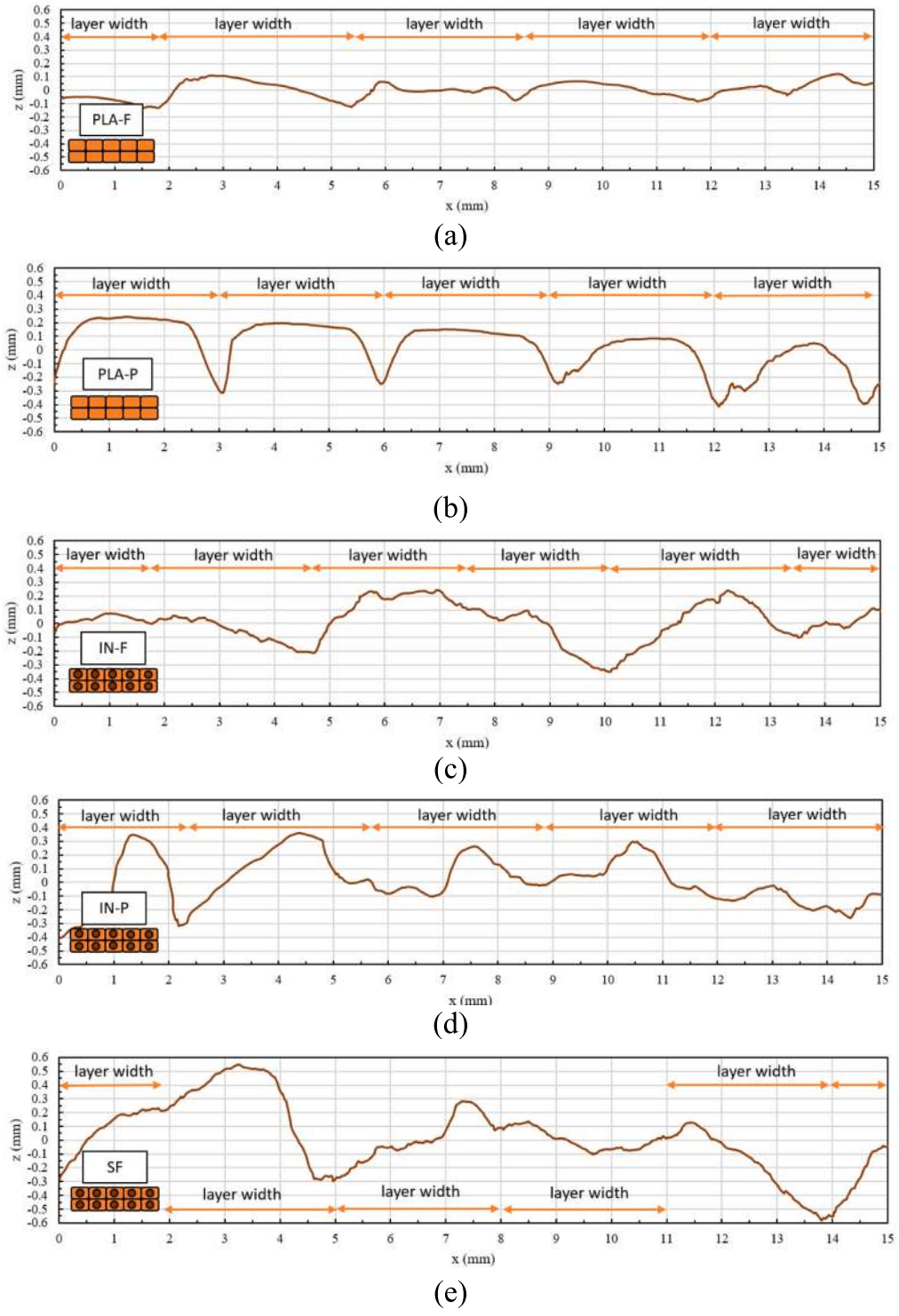

Fig. 13. Surface roughness of printed materials: (a) PLA—F, (b) PLA—P, (c) IN-F, (d) IN-P, and (e) SF.

mm and Ra^{IN-P}=0.159 ± 0.013 mm), but increased by 31.2 % for the semi-finished method (Ra^{SF}=0.223 ± 0.011 mm). Despite this difference, both methods led to a loss of layer uniformity (Fig. 13b, d, and e).

Comparing the two printing methods, although the SF shows higher roughness (Ra^{SF}=0.223 ± 0.011 mm) compared to IN (Ra^{IN-F}=0.142 ± 0.019 mm and Ra^{IN-P}=0.159 ± 0.013 mm), optical microscope analysis revealed noticeable differences in fiber insertion.

To support these results, Fig. 14 presents the SEM images of the fibers and the fiber-matrix interface for each method, offering insight into their respective efficiency. In the SF method, PLA impregnation into the fiber is clearly observable (Fig. 14b), whereas, in the IN-F method, such impregnation is lacking (Fig. 14a). This difference significantly affects the fiber-matrix interface: the IN-F method resulted in a poor interface characterized by a clear and detrimental separation between the fiber and matrix, potentially compromising the composite's mechanical performance (Fig. 14c). Conversely, the SF method yields a more integrated interface, with partial fiber impregnation enhancing the bond between the fiber and matrix (Fig. 14d). However, the presence of unimpregnated fibers in the SF method indicates an incomplete process, particularly for

Table 8
Surface roughness parameters.

Roughness property	PLA-F	PLA-P	IN-F	IN-P	SF
Ra (mm)	0.071 ± 0.000	0.170 ± 0.008	0.142 ± 0.019	0.159 ± 0.013	0.223 ± 0.011
Rq (mm)	0.085 ± 0.000	0.217 ± 0.005	0.177 ± 0.019	0.199 ± 0.017	0.289 ± 0.017
Rz (mm)	0.336 ± 0.026	0.960 ± 0.120	0.725 ± 0.026	0.827 ± 0.061	1.251 ± 0.125

larger diameter yarns, underscoring the necessity for pre-treatment strategies to optimize fiber impregnation and, consequently, the overall composite integrity.

4.3. Analysis of thermal and mechanical performance for in-nozzle and semi-finished approaches

To compare the two investigated approaches in terms of their key mechanical performance, tensile tests were conducted, with the main results summarized in Table 9 and Fig. 15. Both the in-nozzle and semi-finished methods demonstrated improvements in mechanical properties when flax fiber was added, compared to neat PLA. In the case of *in-situ* impregnation using the industrial PLA filament as matrix (IN-F), tensile strength and elastic modulus increased by 34.8 % and 14.1 %, respectively, compared to the neat matrix (PLA—F). For the in-nozzle method using a matrix manufactured from PLA pellets (IN-P), tensile strength and Young's modulus increased by 12.7 % and 2.4 %, respectively, relative to neat PLA (PLA—P). The semi-finished method showed improvements of 29 % in tensile strength and 21.3 % in elastic modulus compared to PLA—P. It is noteworthy the comparison between the two fiber-reinforced methods using the same matrix (PLA—P), the SF method outperformed the IN-P method, with tensile strength and elastic modulus gains of 14.5 % and 18.4 %, respectively.

The tensile strength data for each sample were analyzed using the Anderson-Darling test hypothesis to assess normality (Table 10). The data exhibited a normal distribution, as confirmed by *p*-values higher than the 5 % significance level. A comparison of the normal distribution curves, with a 95 % confidence interval, revealed that none of the results completely overlapped (Fig. 16a, b, and c).

Fig. 17 illustrates the failure modes observed in the tensile samples tested. All samples exhibited brittle rupture in the matrix, initiating with crack propagation across the transverse section. Similar behavior was reported by Santos et al. [11] and Le Duigou [34], who attributed it to imperfect impregnation caused by the twisted yarn structure. The matrix's brittleness, which dominates the composite's overall behavior, leads to reduced reinforcement efficiency in the post-cracking regime of the composite. Additionally, in the post-cracking regime, the flax fiber yarns experienced pullout from the matrix, which further demonstrates the fragility of the fiber-matrix interface.

The effects on the thermal properties of the 3D printed composites were evaluated through DSC testing, with the main results summarized in Table 11 and the corresponding DSC curves illustrated in Fig. 18. The first thermal event observed was the glass transition temperature (T_g), followed by the cold crystallization temperature (T_{cc}), and finally the melting temperature (T_m). The T_g values were recorded between 66.9 °C and 67.5 °C, while the T_{cc} values ranged from 100.1 °C to 101.5 °C, characterized by an exothermic peak. This is likely due to the polymer's limited time to properly crystallize during the rapid cooling rates of FFF, which can reach several tens of degrees per minute [62,63]. The T_m

Table 9
Tensile test results.

Sample	Tensile strength (MPa)	Elastic modulus (GPa)	Tensile strain (%)
PLA-F	35.01 ± 2.39	2.43 ± 0.12	1.64 ± 0.20
PLA-P	40.96 ± 1.70	2.49 ± 0.18	1.87 ± 0.21
IN-F	57.96 ± 5.12	2.68 ± 0.13	2.43 ± 0.29
IN-P	46.15 ± 4.54	2.55 ± 0.16	2.30 ± 0.14
SF	52.84 ± 5.89	3.02 ± 0.28	1.85 ± 0.12

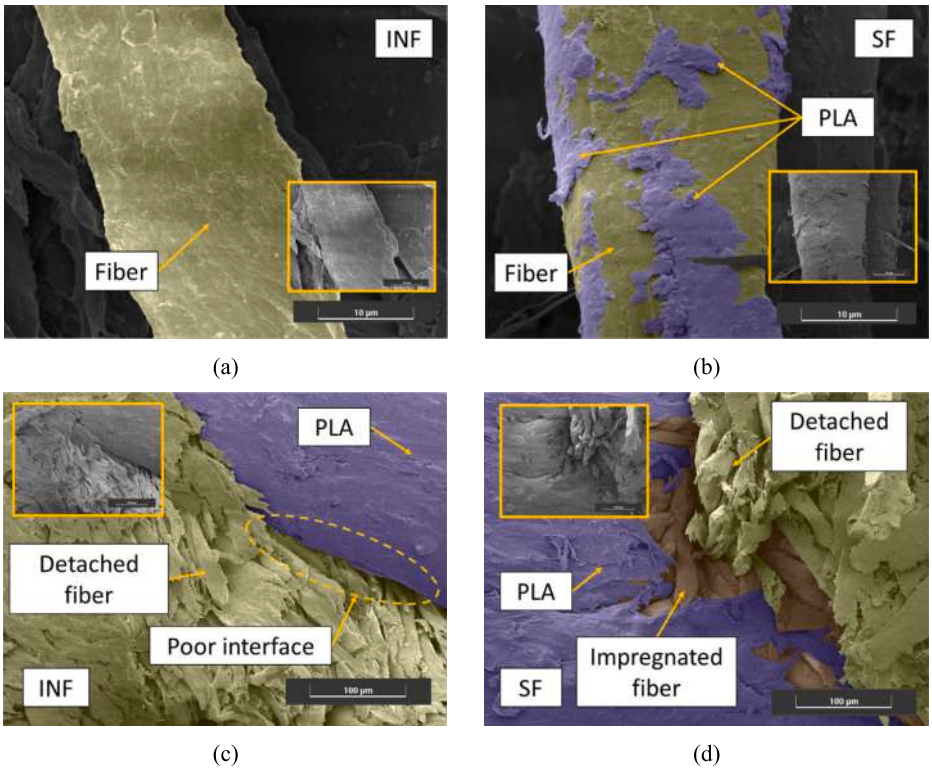

Fig. 14. SEM images of (a) IN-F fiber, (b) SF fiber), (c) IN-F interface, and (d) SF interface. Note: Images have been artificially colored for better visualization.

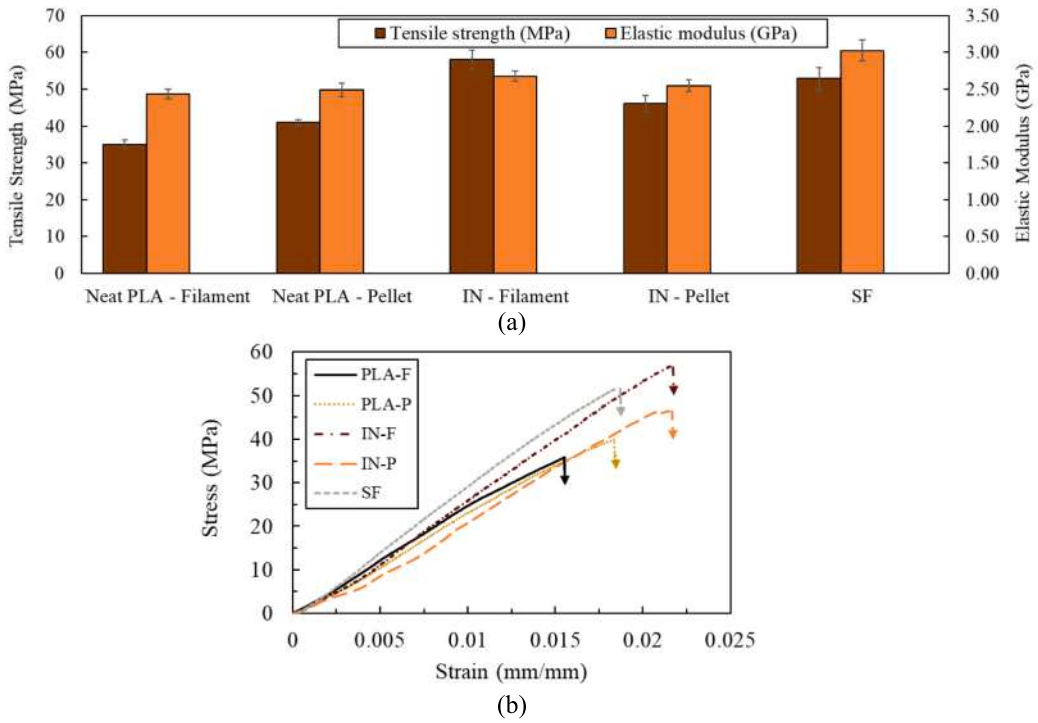

Fig. 15. Overview of the tensile test results: (a) Comparison of tensile strength and elastic modulus (b) stress–strain curves.

Table 10
Anderson-Darling test for tensile strength.

Sample	Mean (MPa)	Standard deviation (MPa)	Number of samples	Anderson Darling parameter	*p*-value
PLA – F	35.01	2.39	5	0.178	0.834
PLA – P	40.96	1.70	5	0.154	0.899
IN – F	57.96	5.12	5	0.248	0.563
IN – P	46.15	4.54	5	0.473	0.126
SF	52.84	5.89	5	0.303	0.414

values were observed within the range of 179.2 °C and 181.9 °C.

The degree of crystallinity (X_c) of the samples was calculated by determining the experimental enthalpies of fusion (ΔH_m) and cold crystallization (ΔH_{cc}), as outlined in Eq. 1. This evaluation was particularly important to assess the actual influence of processing methodologies on the crystallinity of the 3D printed specimens. A comparison of the X_c values revealed an increase in crystallinity when fibers were added: PLA without yarn (PLA—F) had a degree of crystallinity of 47.0 %, while PLA with yarn (IN-F) showed a value of 59.2 %. Similarly, for samples produced through the pellet fusion process, the degree of crystallinity increased from 43 % (PLA—P) to 47.1 % (IN-P) when fibers were incorporated. In both cases, the addition of fibers led to an increase in crystallinity, indicating that higher crystallinity is achieved through natural yarn-reinforcement FFF fiber. Andrzejewski and Nowakowski noted that sufficient fiber reinforcement content fosters crystalline growth on fiber surfaces, promoting a more favorable spherulite structure, which enhances the material's reinforcing properties [64]. However, the SF process exhibited lower crystallinity (37.0 %) compared to the IN-F process (59.2 %), suggesting that lower crystallinity is associated with 3D printing with the SF method. These differences highlight the distinct heating cycles involved in each method. For the *in-situ* process, the heating processing of the composite is limited to the 3D printing stage, whereas an additional thermal cycle is involved for the semi-finished filament fabrication. This extra thermal cycle can reduce crystallinity, as repeated heating and cooling may disturb the ordered molecular regions, preventing polymer chains from realigning into a crystalline structure during cooling. Supporting this observation, Yi et al. demonstrated that biocomposites reinforced with cellulose-based fibers exhibited a progressive reduction in the degree of crystallinity with each thermal cycle [65]. Moreover, although fibers can act as nucleating agents by promoting the formation of crystalline nuclei and enhancing overall crystallinity, reheating above the polymer's melting temperature - such as in the hotend in the SF process - can melt crystalline regions, disrupt polymer chains, and consequently reduce the degree of crystallinity.

5. Conclusions

The research aimed to investigate the differences in physical and mechanical properties resulting from the use of large-diameter natural fiber yarns in FFF 3D-printed PLA, comparing two insertion methods: in-nozzle impregnation during 3D printing (IN) and semi-finished filament (SF). The study found that the SF method resulted in better fiber-matrix bonding, as evidenced by image analysis, and demonstrated superior tensile strength and elastic modulus, with improvements of up to 18.4 % over the IN method. Additionally, the SF method allowed for faster printing speeds of up to 400 mm/min, compared to the 300 mm/min limit of the IN method. The presence of fibers also increased the degree of crystallinity, though this was reduced after repeated thermal cycles, which disrupted the crystalline regions.

The study's limitations include the lack of exploration of yarn pretreatments and multi-filament strategies for large-scale applications. Future developments should address these gaps by improving impregnation quality, investigating the effect of exposure time to the heated nozzle on impregnation, and optimizing inter-ply strength through detailed mechanical analyses. These efforts will be crucial for enhancing composite performance and fully understanding the impact of processing parameters. Despite these limitations, the results highlight the potential of the SF method for advancing natural fiber-reinforced composites in FFF 3D printing. The demonstrated improvements in mechanical properties and process efficiency pave the way for innovative and sustainable application scenarios.

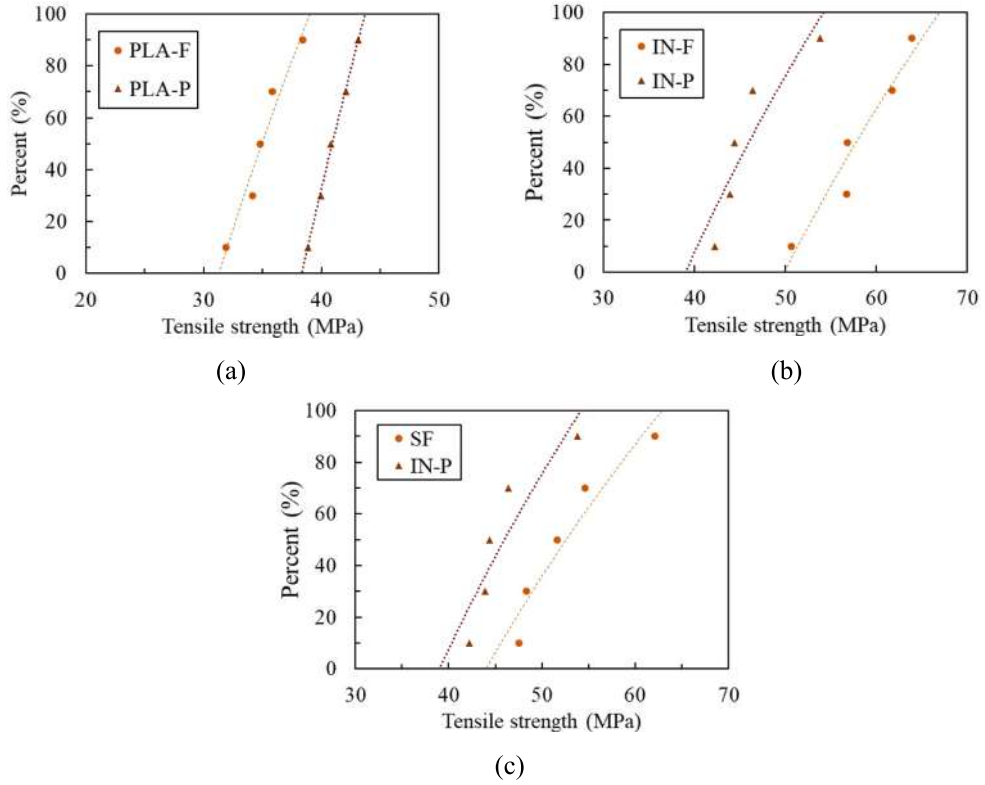

Fig. 16. Normal probability graphic analysis: (a) neat PLA-F and PLA—P, (b) the in-nozzle method IN-F and IN-P, and (c) different methods with the same matrix (IN-P and SF).

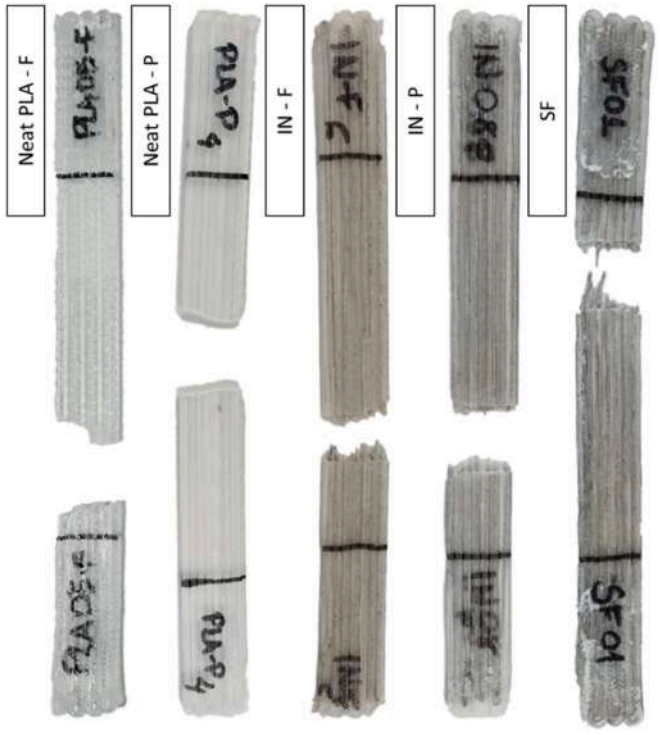

Fig. 17. Example of failure modes of the tensile samples.

Table 11
Thermal properties of different composites evaluated with DSC.

Properties	PLA-F	IN-F	PLA-P	IN-P	SF
T_g - Glass transition temperature (°C)	67.1	66.0	66.9	67.5	65.9
T_{cc} – Cold crystallization temperature (°C)	101.5	100.1	100.9	102.6	100.4
ΔH_{cc} - Cold crystallization enthalpy (J/g)	86.3	66.7	94.3	56.6	102.8
T_m - Melting temperature (°C)	181.9	181.2	179.2	180.6	181.6
ΔH_m – Melting enthalpy (J/g)	130.0	121.8	134.3	100.4	137.2
X_c – Degree of crystallinity (%)	47.0	59.2	43.0	47.1	37.0

Fundings

This study was financed in part by the *Coordenação de Aperfeiçoamento de Pessoal de Nível Superior* – Brazil (CAPES) – Finance Code 001 and CAPES PrInt 88887.889279/2023-00. Also, this study was financed in part by Brazilian funding agencies FAPERJ and CNPq.

CRediT authorship contribution statement

Natália V. dos Santos: Writing – original draft, Methodology, Investigation, Data curation, Conceptualization. **Alberto Giubilini:** Writing – review & editing, Supervision, Investigation. **Daniel Carlos T. Cardoso:** Writing – review & editing, Supervision, Conceptualization. **Paolo Minetola:** Writing – review & editing, Supervision, Resources.

Declaration of competing interest

The authors declare that they have no known competing financial interests or personal relationships that could have appeared to influence the work reported in this paper.

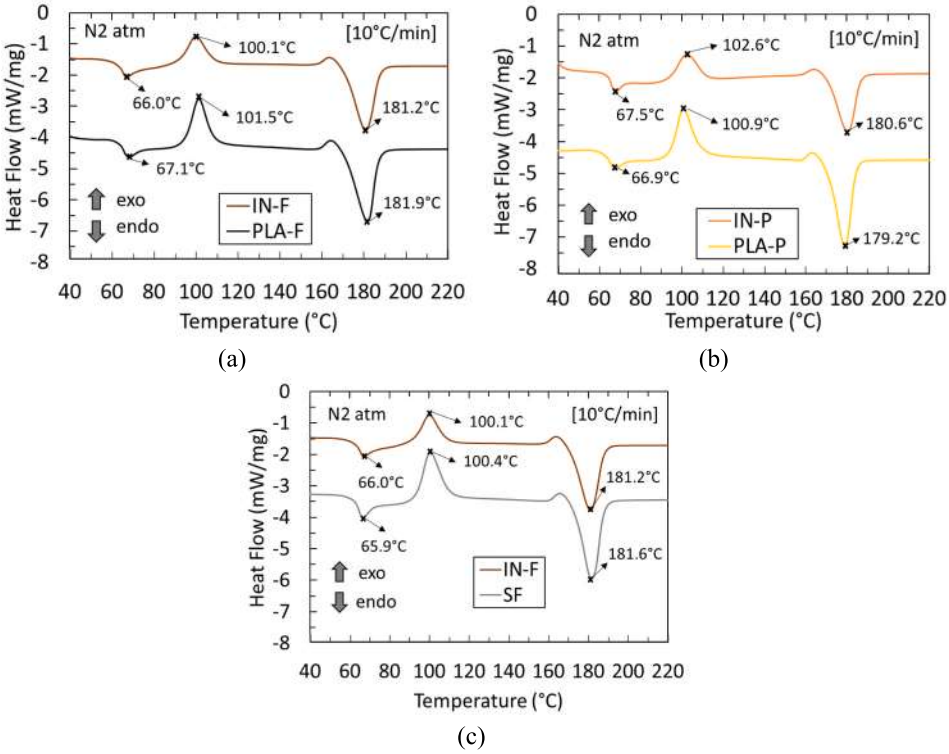

Fig. 18. Comparative DSC scans of the 3D printing methods: (a) IN-F and PLA—F, (b) IN-P and PLA—P, (c) IN-F and SF.

Data availability

Data will be made available on request.

Acknowledgments

All testing was conducted at the Laboratory of Structures and Materials of the Pontifical Catholic University of Rio de Janeiro and at the Reverse Laboratory and the Rapid Manufacturing Laboratory of Politecnico di Torino.

References

[1] J. Kechagias, S. Zaoutsos, Effects of 3D-printing processing parameters on FFF parts' porosity: outlook and trends, Mater. Manuf. Process. 39 (2024) 804–814, https://doi.org/10.1080/10426914.2024.2304843.
[2] I. Buj-Corral, A. Bagheri, M. Sivatte-Adroer, Effect of printing parameters on dimensional error, surface roughness and porosity of FFF printed parts with grid structure, Polymers (Basel) 13 (2021) 1213, https://doi.org/10.3390/polym13081213.
[3] I. Buj-Corral, X. Sánchez-Casas, C.J. Luis-Pérez, Analysis of AM parameters on surface roughness obtained in PLA parts printed with FFF technology, Polymers (Basel) (2021) 13, https://doi.org/10.3390/polym13142384.
[4] J.D. Kechagias, Surface roughness assessment of ABS and PLA filament 3D printing parts: structural parameters experimentation and semi-empirical modelling, Int. J. Adv. Manuf. Technol. 134 (2024) 1935–1946, https://doi.org/10.1007/s00170-024-14232-0.
[5] A. Plymill, R. Minneci, D. Alexander Greeley, J. Gritton, D. Greeley, R. Minneci, et al., Graphene and Carbon Nanotube PLA Composite Feedstock Development for Fused Deposition Modeling, 2016.
[6] M.-A. Arsène, H. Savastano Jr., S.M. Allameh, K. Ghavami, W.O. Soboyejo, Cementitious composites reinforced with vegetable fibers, in: Proceedings of the 1st Interamerican Conference on Non-Conventional Materials and Technologies in the Eco-Construction and Infrastructure (IAC-NOCMAT), 2003, pp. 13–16.
[7] P. Wambua, J. Ivens, I. Verpoest, Natural fibres: can they replace glass in fibre reinforced plastics? Compos. Sci. Technol. 63 (2003) 1259–1264, https://doi.org/10.1016/S0266-3538(03)00096-4.
[8] J.S.S. Neto, R.A.A. Lima, D.K.K. Cavalcanti, J.P.B. Souza, R.A.A. Aguiar, M. D. Banea, Effect of chemical treatment on the thermal properties of hybrid natural fiber-reinforced composites, J. Appl. Polym. Sci. 136 (2019) 1–13, https://doi.org/10.1002/app.47154.
[9] A.K. Mohanty, M. Misra, L.T. Drzal, Natural Fibers, Biopolymers, and Biocomposites, Taylor & Francis, 2005.
[10] W.H. Morrison, D.D. Archibald, H.S.S. Sharma, D.E. Akin, Chemical and physical characterization of water- and dew-retted flax fibers, Ind. Crops Prod. 12 (2000) 39–46, https://doi.org/10.1016/S0926-6690(99)00044-8.
[11] N.V. Santos, D.C.T. Cardoso, 3D printing of vegetable yarn-reinforced polymer components, J. Clean. Prod. (2023) 415, https://doi.org/10.1016/j.jclepro.2023.137870.
[12] S.J. Eichhorn, C.A. Baillie, N. Zafeiropoulos, L.Y. Mwaikambo, M.P. Ansell, A. Dufresne, et al., Current international research into cellulosic fibres and composites, J. Mater. Sci. 36 (2001) 2107–2131, https://doi.org/10.1023/A:1017512029696.
[13] M.N. Ahmad, M.R. Ishak, M. Mohammad Taha, F. Mustapha, Z. Leman, A review of natural fiber-based filaments for 3D printing: filament fabrication and characterization, Materials 16 (2023), https://doi.org/10.3390/ma16114052.
[14] A. Romani, R. Suriano, M. Levi, Biomass waste materials through extrusion-based additive manufacturing: a systematic literature review, J. Clean. Prod. (2023) 386, https://doi.org/10.1016/j.jclepro.2022.135779.
[15] F.S. Shahar, M.T. Hameed Sultan, S.N.A. Safri, M. Jawaid, A.R. Abu Talib, A. A. Basri, et al., Physical, thermal and tensile behaviour of 3D printed kenaf/PLA to suggest its usability for ankle–foot orthosis – a preliminary study, Rapid Prototyp. J. 28 (2022) 1573–1588, https://doi.org/10.1108/RPJ-08-2021-0207.
[16] Y. Tao, P. Li, J. Zhang, S. Wang, S.Q. Shi, F. Kong, A review of fused filament fabrication of continuous natural fiber reinforced thermoplastic composites: techniques and materials, Polym. Compos. 44 (2023) 8200–8222, https://doi.org/10.1002/pc.27477.
[17] W.K. Durfee, P.A. Iaizzo, Medical applications of 3D printing, in: Engineering in Medicine: Advances and Challenges, Elsevier, 2018, pp. 527–543, https://doi.org/10.1016/B978-0-12-813068-1.00021-X.
[18] A.M. Pringle, M. Rudnicki, J.M. Pearce, Wood furniture waste-based recycled 3-D printing filament, For. Prod. J. 68 (2018) 86–95, https://doi.org/10.13073/FPJ-D-17-00042.
[19] F. Yang, J. Zeng, H. Long, J. Xiao, Y. Luo, J. Gu, et al., Micrometer copper-zinc alloy particles-reinforced wood plastic composites with high gloss and antibacterial properties for 3D printing, Polymers (Basel) (2020) 12, https://doi.org/10.3390/polym12030621.
[20] N.D. Sanandiya, C. Ottenheim, J.W. Phua, A. Caligiani, S. Dritsas, J.G. Fernandez, Circular manufacturing of chitinous bio-composites via bioconversion of urban refuse, Sci. Rep. (2020) 10, https://doi.org/10.1038/s41598-020-61664-1.
[21] M. Sauerwein, J. Zlopasa, Z. Doubrovski, C. Bakker, R. Balkenende, Reprintable paste-based materials for additive manufacturing in a circular economy, Sustainability (Switzerland) 12 (2020) 1–15, https://doi.org/10.3390/su12198032.
[22] A. Cislaghi, P. Sala, G. Borgonovo, C. Gandolfi, G.B. Bischetti, Towards more sustainable materials for geo-environmental engineering: the case of geogrids, Sustainability (Switzerland) 13 (2021) 1–21, https://doi.org/10.3390/su13052585.

[23] A. Romani, V. Rognoli, M. Levi, Design, materials, and extrusion-based additive manufacturing in circular economy contexts: from waste to new products, Sustainability (Switzerland) (2021) 13, https://doi.org/10.3390/su13137269.
[24] V. Figueroa-Velarde, T. Diaz-Vidal, E.O. Cisneros-López, J.R. Robledo-Ortiz, E. J. López-Naranjo, P. Ortega-Gudiño, et al., Mechanical and physicochemical properties of 3d-printed agave fibers/poly(lactic) acid biocomposites, Materials (2021) 14, https://doi.org/10.3390/ma14113111.
[25] A. Haryati, N. Razali, M. Petrů, M. Taha, N. Muhammad, R.A. Ilyas, Effect of chemically treated kenaf fibre on mechanical and thermal properties of PLA composites prepared through fused deposition modeling (FDM), Polymers (Basel) (2021) 13, https://doi.org/10.3390/polym13193299.
[26] H. Liu, H. He, X. Peng, B. Huang, J. Li, Three-dimensional printing of poly(lactic acid) bio-based composites with sugarcane bagasse fiber: effect of printing orientation on tensile performance, Polym. Adv. Technol. 30 (2019) 910–922, https://doi.org/10.1002/pat.4524.
[27] I. Fekete, F. Ronkay, L. Lendvai, Highly toughened blends of poly(lactic acid) (PLA) and natural rubber (NR) for FDM-based 3D printing applications: the effect of composition and infill pattern, Polym. Test. (2021) 99, https://doi.org/10.1016/j.polymertesting.2021.107205.
[28] A. Dey, M.M. Rahman, N. Yodo, D. Grewell, Development of biocomposite filament for fused filament fabrication from soy hulls and soy protein isolate, Mater. Today Commun. (2023) 34, https://doi.org/10.1016/j.mtcomm.2023.105316.
[29] S. Pervaiz, T.A. Qureshi, G. Kashwani, S. Kannan, 3D printing of fiber-reinforced plastic composites using fused deposition modeling: a status review, Materials 14 (2021) 4520, https://doi.org/10.3390/ma14164520.
[30] T. Wang, N. Li, G. Link, J. Jelonnek, J. Fleischer, J. Dittus, et al., Load-dependent path planning method for 3D printing of continuous fiber reinforced plastics, Compos. Part A Appl. Sci. Manuf. (2021) 140, https://doi.org/10.1016/j.compositesa.2020.106181.
[31] H. Zhang, X. Lei, Q. Hu, S. Wu, M. Aburaia, J. Gonzalez-Gutierrez, et al., Hybrid printing method of polymer and continuous fiber-reinforced thermoplastic composites (CFRTPCs) for pipes through double-nozzle five-Axis printer, Polymers (Basel) (2022) 14, https://doi.org/10.3390/polym14040819.
[32] H. Zhang, D. Liu, T. Huang, Q. Hu, H. Lammer, Three-dimensional printing of continuous flax fiber-reinforced thermoplastic composites by five-axis machine, Materials (2020) 13, https://doi.org/10.3390/ma13071678.
[33] G. Ginoux, X. Wu, C. Laqraa, D. Soulat, J. Paux, M. Ferreira, et al., Continuous additive manufacturing of hemp yarn-reinforced biocomposites with improved impregnation method, Compos. Sci. Technol. 251 (2024) 110561, https://doi.org/10.1016/j.compscitech.2024.110561.
[34] A. Le Duigou, A. Barbé, E. Guillou, M. Castro, 3D printing of continuous flax fibre reinforced biocomposites for structural applications, Mater. Des. 180 (2019) 107884, https://doi.org/10.1016/j.matdes.2019.107884.
[35] A. Le Duigou, P. Davies, C. Baley, Exploring durability of interfaces in flax fibre/epoxy micro-composites, Compos. Part A Appl. Sci. Manuf. 48 (2013) 121–128, https://doi.org/10.1016/j.compositesa.2013.01.010.
[36] T. Fruleux, M. Castro, P. Sauleau, R. Matsuzaki, A. Le Duigou, Matrix stiffness: a key parameter to control hydro-elasticity and morphing of 3D printed biocomposite, Compos. Part A Appl. Sci. Manuf. (2022) 156, https://doi.org/10.1016/j.compositesa.2022.106882.
[37] T. Fruleux, M. Castro, D. Correa, K. Wang, R. Matsuzaki, A. Le Duigou, Geometric limitations of 3D printed continuous flax-fiber reinforced biocomposites cellular lattice structures, Composites Part C: Open Access (2022) 9, https://doi.org/10.1016/j.jcomc.2022.100313.
[38] P. Cheng, K. Wang, X. Chen, J. Wang, Y. Peng, S. Ahzi, et al., Interfacial and mechanical properties of continuous ramie fiber reinforced biocomposites fabricated by in-situ impregnated 3D printing, Ind. Crop. Prod. 170 (2021) 113760, https://doi.org/10.1016/j.indcrop.2021.113760.
[39] P. Cheng, K. Wang, X. Chen, A. Le Duigou, Y. Peng, W. Wen, Compressive property and shape memory effect of 3D printed continuous ramie fiber reinforced biocomposite corrugated structures, Smart Mater. Struct. 31 (2022) 124003, https://doi.org/10.1088/1361-665x/ac95e4.
[40] P. Cheng, Y. Peng, K. Wang, A. Le Duigou, S. Yao, C. Chen, Quasi-static penetration property of 3D printed woven-like ramie fiber reinforced biocomposites, Compos. Struct. 303 (2023) 116313, https://doi.org/10.1016/j.compstruct.2022.116313.
[41] J. Suteja, H. Firmanto, A. Soesanti, C. Christian, Properties investigation of 3D printed continuous pineapple leaf fiber-reinforced PLA composite, J. Thermoplast. Compos. Mater. 35 (2022) 2052–2061, https://doi.org/10.1177/0892705720945371.
[42] R. Matsuzaki, M. Ueda, M. Namiki, H. Tae-Kun Jeong, K. Horiguchi, A. Taishi Nakamura, YH, Three-Dimensional Printing of Continuous-Fiber Composites by In-Nozzle Impregnation, 2016.
[43] Y. Long, Z. Zhang, K. Fu, Y. Li, Efficient plant fibre yarn pre-treatment for 3D printed continuous flax fibre/poly(lactic) acid composites, Compos. B Eng. (2021) 227, https://doi.org/10.1016/j.compositesb.2021.109389.
[44] R. Cai, H. Lin, P. Cheng, Z. Zhang, K. Wang, Y. Peng, et al., Investigation on dynamic strength of 3D-printed continuous ramie fiber reinforced biocomposites at various strain rates using machine learning methods, Polym. Compos. 43 (2022) 5235–5249, https://doi.org/10.1002/pc.26816.
[45] S. Terekhina, S. Egorov, T. Tarasova, I. Skornyakov, L. Guillaumat, M.L. Hattali, In-nozzle impregnation of continuous textile flax fiber/polyamide 6 composite during FFF process, Compos. Part A Appl. Sci. Manuf. (2022) 153, https://doi.org/10.1016/j.compositesa.2021.106725.
[46] O. Rivero-Romero, I. Barrera-Fajardo, J. Unfried-Silgado, Effects of printing parameters on fiber eccentricity and porosity level in a thermoplastic matrix composite reinforced with continuous banana fiber fabricated by FFF with in situ impregnation, Int. J. Adv. Manuf. Technol. 125 (2023) 1893–1901, https://doi.org/10.1007/s00170-022-10799-8.
[47] X. Wu, G. Ginoux, J. Paux, S. Allaoui, Damage and fracture studies of continuous flax fiber-reinforced composites 3D printed by in-nozzle impregnation additive manufacturing, Int. J. Damage Mech. (2024), https://doi.org/10.1177/10567895241279845.
[48] J. Pereira de Moraes, L. Nunes Martins de Lima, R. Miranda Barbosa, Yarns and weaves: the know-how and the orality of spinners and weavers in Xixá, História Oral 26 (2023) 30–50, https://doi.org/10.51880/ho.v26i2.1373.
[49] V.C.B. Camargo, B. Almada-Lobo, F.M.B. Toledo, Integrated lotsizing, scheduling and blending decisions in the spinning industry, Pesquisa Operacional (2021) 41, https://doi.org/10.1590/0101-7438.2021.041s1.00233486.
[50] P. Zhuo, S. Li, I.A. Ashcroft, A.I. Jones, Material extrusion additive manufacturing of continuous fibre reinforced polymer matrix composites: a review and outlook, Compos. B Eng. (2021) 224, https://doi.org/10.1016/j.compositesb.2021.109143.
[51] N. Li, Y. Li, S. Liu, Rapid prototyping of continuous carbon fiber reinforced polylactic acid composites by 3D printing, J. Mater. Process. Technol. 238 (2016) 218–225, https://doi.org/10.1016/j.jmatprotec.2016.07.025.
[52] G. Chabaud, M. Castro, C. Denoual, A. Le Duigou, Hygromechanical properties of 3D printed continuous carbon and glass fibre reinforced polyamide composite for outdoor structural applications, Addit. Manuf. 26 (2019) 94–105, https://doi.org/10.1016/j.addma.2019.01.005.
[53] R. Matsuzaki, T. Nakamura, K. Sugiyama, M. Ueda, A. Todoroki, Y. Hirano, et al., Effects of set curvature and fiber bundle size on the printed radius of curvature by a continuous carbon fiber composite 3D printer, Addit. Manuf. 24 (2018) 93–102, https://doi.org/10.1016/j.addma.2018.09.019.
[54] A.K. Mohanty, M. Misra, L.T. Drzal, Natural Fibers, Biopolymers, and Biocomposites, Taylor & Francis, 2005.
[55] 3D DEVO, Netherlands, 2024.
[56] D. Johnson, Filament Extrusion Using Recycled Materials, Halmstad University, 2020.
[57] British Standards Institution, British Standards Institution. BS EN ISO 4288:1998: Geometric product specifications (GPS) - surface texture: profile method: rules and procedures for the assessment of surface texture, British Standards Institution, 1998.
[58] ASTM. ASTM D3039 / D3039M - Standard Test Method for Tensile Properties of Polymer Matrix Composite Materials. Annual Book of ASTM Standards n.d.;15.03. https://doi.org/10.1520/D3039_D3039M-17.
[59] ASTM, ASTM D3418 - Standard Test Method for Transition Temperatures of Polymers by Differential Scanning Calorimetry, 2021.
[60] Kong Y, Hay JN. The Measurement of the Crystallinity of Polymers by DSC. n.d.
[61] C. Zhang, Q. Lan, T. Zhai, S. Nie, J. Luo, W. Yan, Melt crystallization behavior and crystalline morphology of polylactide/poly(ε-caprolactone) blends compatibilized by lactide-caprolactone copolymer, Polymers (Basel) (2018) 10, https://doi.org/10.3390/polym10111181.
[62] E. Lannunziata, G. Colucci, P. Minetola, A. Giubilini, Effect of annealing treatment and infill percentage on 3D-printed PEEK samples by fused filament fabrication, Int. J. Adv. Manuf. Technol. 131 (2024) 5209–5222, https://doi.org/10.1007/s00170-024-13347-8.
[63] J. Zhang, E. Vasiliauskaite, A. De Kuyper, C. De Schryver, F. Vogeler, F. Desplentere, et al., Temperature analyses in fused filament fabrication: from filament entering the hot-end to the printed parts, 3D Print Addit. Manuf. 9 (2022) 132–142, https://doi.org/10.1089/3dp.2020.0339.
[64] J. Andrzejewski, M. Nowakowski, Development of toughened flax fiber reinforced composites. Modification of poly(lactic acid)/poly(butylene adipate-co-terephthalate) blends by reactive extrusion process, Materials (2021) 14, https://doi.org/10.3390/ma14061523.
[65] C. Yi, L. Tian, F. Tang, L. Wang, H. Zou, W. Xu, Crystalline transition behavior of sisal in cycle process, Polym. Compos. 31 (2010) 933–938, https://doi.org/10.1002/pc.20885.